Received: 14 June 2018 | Revised: 12 March 2019 | Accepted: 18 March 2019

DOI: 10.1002/rra.3429

RESEARCH ARTICLE

WILEY

# Spatio-temporal variability in underwater light climate in a turbid river-floodplain system: Driving factors and estimation using Secchi disc

Gisela Mayora | Melina Devercelli

Instituto Nacional de Limnología (INALI-UNL-CONICET), Paraje El Pozo, Ciudad Universitaria, Santa Fe, Argentina

**Correspondence**
Gisela Mayora, Instituto Nacional de Limnología (INALI-UNL-CONICET), Paraje El Pozo, Ciudad Universitaria, Santa Fe C.P. 3000, Argentina.
Email: gpmayora@inali.unl.edu.ar

**Funding information**
Agencia Nacional de Promoción Científica y Tecnológica; Consejo Nacional de Investigaciones Científicas y Técnicas

## Abstract

The underwater light climate has important effects on primary producers. The aim of this research was to evaluate its variability in a turbid river-floodplain system. Photosynthetically active radiation (PAR) was measured in the Middle Paraná River during different hydrological phases to (a) analyse the photosynthetically active radiation attenuation coefficient ($k$) and euphotic depth ($Z_{eu}$) as well as their associations with optically active components and (b) develop and evaluate indices and regression models based on Secchi disc (SD) measurements to estimate $k$ and $Z_{eu}$. Values of $k$ were higher in the fluvial system than in the floodplain and during low-water stage than high-water stage. Particulate components controlled the light climate variability. Chromophoric dissolved organic matter and chlorophyll-*a* had significant effects during floods. The estimation of $k$ and $Z_{eu}$ was sensitive to temporal but not to spatial variations. The highest prediction accuracy was observed when using specific non-linear regressions for each hydrological phase, especially for $Z_{eu}$ estimation (low stage: $k = 1.76 \times SD^{-0.80}$, $Z_{eu} = 2.62 \times 1/SD^{-0.80}$; high stage: $k = 2.04 \times SD^{-0.53}$, $Z_{eu} = 2.26 \times 1/SD^{-0.53}$). The indices $k \times SD$ and $Z_{eu}/SD$ were significantly different from those proposed for clear water environments. It is concluded that temporal variations should be considered when estimating $k$ and $Z_{eu}$ in turbid river-floodplain systems because of the temporal heterogeneity in optically active components. Considering that ecological implication of the light climate depends on $Z_{eu}$:depth ratio, we propose to estimate $Z_{eu}$ instead of $k$. Finally, indices proposed for clear water environments are not recommended to be applied to turbid environments.

**KEYWORDS**

CDOM, chlorophyll-*a*, floodplain river, hydrological regime, PAR, Paraná River system, Secchi disc, turbidity

## 1 | INTRODUCTION

River-floodplain systems are subject to marked temporal and spatial variability in hydrological conditions (Tockner, Pusch, Borchardt, & Lorang, 2010). Variations in hydrology are accompanied by pronounced changes in the optically active components of the water column (Costa, Novo, & Telmer, 2013; Zhang, Zhang, Ma, Feng, & Le, 2007). This has implications for both the underwater light climate and its evaluation from Secchi disc depth (SD) measurements (Padial & Thomaz, 2008). Light climate is defined by the euphotic depth ($Z_{eu}$), which is inversely associated with the vertical attenuation of photosynthetically active radiation (PAR). Attenuation of PAR is

  

regulated by light scattering due to particulate matter, that is, phytoplankton and nonpigmented particulate matter and by light absorption due to particulate and dissolved matter, particularly chromophoric dissolved organic matter (CDOM). Light climate plays an important role in regulating primary productivity in the water column (Piedade et al., 2010; Zhang et al., 2016), which highlights the importance of its correct evaluation.

Previous studies have shown a decrease in suspended particulate matter and an increase in CDOM and phytoplankton biomass from the main channel (MC) towards the most isolated floodplain water bodies (Mayora, Devercelli, & Frau, 2016; Unrein, 2002; Zalocar de Domitrovic, Devercelli, & García de Emiliani, 2007). The spatial differences are more evident during isolation periods due to the effects of local driving forces (Maine, Suñe, & Bonetto, 2004; Roberto, Santana, & Thomaz, 2009; Thomaz, Bini, & Bozelli, 2007). However, exceptions to this general rule can occur. Under certain circumstances, turbidity of floodplain lakes resembles the high values of the MC during low-water stage whereas noticeable differences occur during floods (Mayora, Devercelli, & Giri, 2013). This indicates that the factors regulating the concentration of suspended particles may be highly variable among environments even during periods of high hydrological connectivity. In lotic environments, suspended sediment peaks are generally associated to rainfall events in the watershed; whereas in shallow lakes, they are generally associated with wind-driven resuspension (Liu, Zhang, Yin, Wang, & Qin, 2013; Shi, Zhang, Liu, Wang, & Qin, 2014).

PAR attenuation coefficients ($k$), and $Z_{eu}$ can be accurately calculated from vertical profiles of underwater PAR irradiance by using underwater quantum sensors (Liu et al., 2013; Padial & Thomaz, 2008). In addition, SD is widely used to estimate $k$ and $Z_{eu}$ due to the ease of its measurement (Cardoso et al., 2017; Pineda et al., 2017; Zanco, Pineda, Bortolini, Jati, & Rodrigues, 2017). The significant correlations between SD and $k$, and between SD and $Z_{eu}$, allow for the use of regression models (Padial & Thomaz, 2008; Zhang, Liu, Yin, Wang, & Qin, 2012) and indices, which emerge from the product $k \times SD$ and the ratio $Z_{eu}/SD$ (Koenings & Edmundson, 1991). However, SD is subject to limitations because their correlations with $k$ and $Z_{eu}$ are influenced by the partitioning of PAR attenuation between the processes of absorption and scattering. The use of equations developed from environments with a higher ratio of PAR scattering to absorption increases the risk of overestimating $Z_{eu}$; whereas the use of equations developed from environments with a lower ratio of PAR scattering to absorption increases the risk of underestimating $Z_{eu}$ (Koenings & Edmundson, 1991).

Although it has long been known that the balance between scattering and absorption of PAR influences the relations between SD and $k$, and between SD and $Z_{eu}$ (Effler, 1985), SD is widely applied to evaluate light climate variability in river-floodplain systems without validating if the relations are constant in space and time (Cardoso et al., 2017; Mayora et al., 2013; Pineda et al., 2017; Zanco et al., 2017). As a result, this research aims to evaluate the main components driving the variability in light climate in a turbid river-floodplain system and the feasibility of evaluating it from SD. The MC of the Middle Paraná River and floodplain water bodies were sampled during high- and low-water stages to (a) analyse the variability in $k$ and $Z_{eu}$ as well as their associations with the main optically active components; (b) develop SD-based indices and regression models to evaluate the feasibility of estimating $k$ and $Z_{eu}$ from them; and (c) compare the developed indices to those proposed for other environments. We hypothesized that the estimations of $k$ and $Z_{eu}$ using SD are sensitive to the effects of space and time because of the variations in the balance between PAR scattering and absorption. A greater influence of the spatial gradient was expected to occur during low-water stage.

## 2 | MATERIALS AND METHODS

### 2.1 | Study sites

The Paraná River drains an area of $3.1 \times 10^6$ km$^2$ (Figure 1), and it is the second largest river in South America after the Amazon. The middle stretch of the river extends from its confluence with the Paraguay River (27° 29' S; 58° 50' W) to the city of Diamante (Argentina; 32° 4' S; 60° 32' W). It is characterized by high turbidity (concentration of suspended particulate matter = 20 to 310 mg $L^{-1}$, Bonetto et al., 1994), and SD is usually low. Nearly 90% of the suspended particulate matter is supplied, through the Paraguay River, via the Bermejo River (Amsler & Drago, 2009). The load of particulate matter is predominantly composed of silts and clays (Amsler, Drago, & Paira, 2007). Different geochemical approaches indicate that the particles preserve the chemical signature of rock sources during their transport (Campodonico, García, & Pasquini, 2016). Nearly 75% of the water discharge is from the Upper Paraná River. About 50% of the water flows through a well-defined MC and the remainder through large anabranches.

The Middle Paraná River has a 10 to 50 km wide floodplain (13,000 km$^2$) along its right bank, which includes lakes (mean area: 0.32 km$^2$, mean maximum depth: 1.46 m) with variable degrees of connectivity to the fluvial system as well as secondary channels that constitute the floodplain drainage network (Drago, 2007). Gallery forests grow on the levees, and extensive pastures cover low lying areas. Among aquatic macrophytes, emergent and free-floating species stand out for their biomass and areal coverage of water bodies (Sabattini & Lallana, 2007). Vegetation increases floodplain roughness and reduces current velocity. Therefore, the floodplain acts as a storage area for particulate matter carried by the river during high flows (Maine et al., 2004). The turbulence of lotic environments and the shallowness of floodplain lakes allows for a continued vertical mixing and prevents the formation of discontinuities in water quality through the water column (Drago, 2007).

The studied sites and periods were selected to represent the spatio-temporal heterogeneity of the Middle Paraná River system (Devercelli, Scarabotti, Mayora, Schneider, & Giri, 2016). To capture the temporal variability, four surveys, each lasting 10 days, were conducted during low-water stages (November–December 2013, March–April 2014) and high-water stages (September 2015, February–March

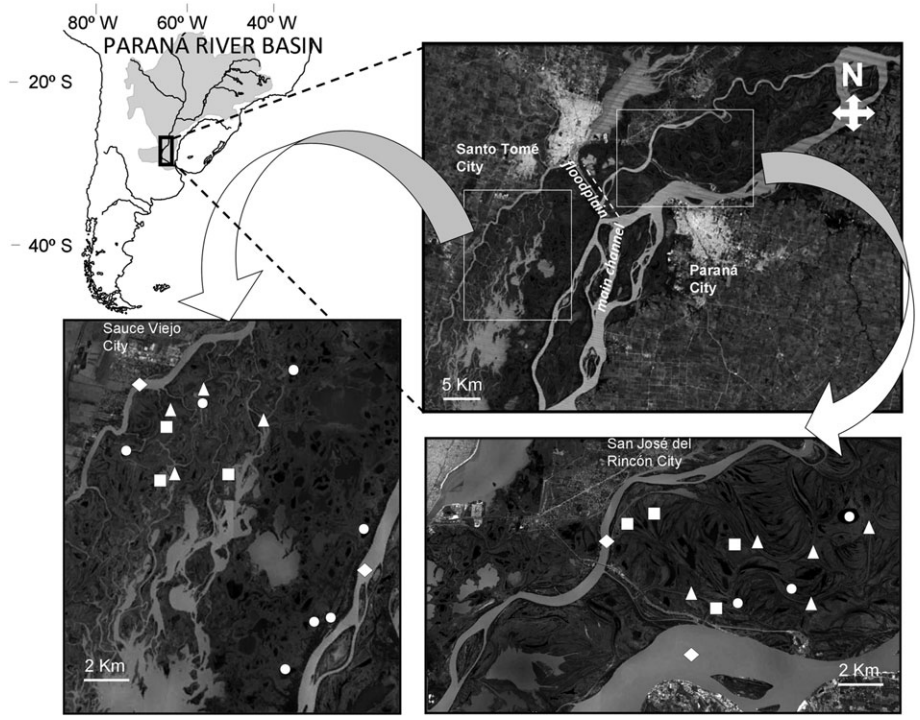


**FIGURE 1** Location of the study area. Sampling sites are indicated with rhombuses (main channel and anabranches of the Middle Paraná River), triangles (secondary channels), squares (lakes permanently connected to the fluvial system), and circles (lakes temporarily connected to the fluvial system)

2016). To consider the spatial heterogeneity, different types of environment were sampled: the MC and three anabranches (MC), nine secondary channels (SC), seven lakes permanently connected to the fluvial system (LPC), and 10 lakes temporarily connected to the fluvial system (LTC; Figure 1).

## 2.2 | Samplings and laboratory analyses

Sampling was undertaken at the centre of the lotic environments and in the pelagic zone of the lakes. SD was measured in situ using a standard disc of 30 cm in diameter with alternating black and white quarters. Measurements of 15-s averages (approximately 60 readings) of underwater PAR (μmol $s^{-1}$ $m^{-2}$) were recorded using a LI-COR® quantum meter LI-250 connected to a LI-193 Spherical Quantum Sensor (Lincoln, NE, USA). Measurements were made at intervals of 20 cm from the subsurface of the water column to 60 cm depth, except in water bodies shallower than 60 cm where PAR was measured to the bottom.

Subsurface water samples were collected in duplicate, transported on ice and in darkness to the laboratory, and processed within 24 hr after collection. Turbidity (formazin turbidity units, FTU) was spectrophotometrically estimated at 450-nm wavelength with a HACH DR 2000 spectrophotometer and used as a proxy for the concentration of suspended particulate matter (Rügner, Schwientek, Beckingham, Kuch, & Grathwohl, 2013). A variable volume of water (300–1,200 mL) was filtered through Whatman GF/C glass-fibre filters, which were stored at −20°C. Chlorophyll-*a* was extracted from the filters with acetone (90%). Extracts were filtered and then spectrophotometrically measured at 750 and 664 nm, and at 665 and 750 nm after acidification with HCl 0.1 M according to Lorenzen's method (APHA, 2005). Filtered water samples were passed through Millipore filters (pore size: 0.45 μm) for the analysis of CDOM (water colour, mg $L^{-1}$ platinum–cobalt (Pt–Co)) at 455 nm using a spectrophotometer HACH DR 5000 and filtered Milli-Q water as a baseline. The ratio of (turbidity × 10)/colour was used as an index (Turb/Col) indicative of the ratio of scattering to absorption of PAR (Koenings & Edmundson, 1991).

## 2.3 | Data analyses

Vertical profiles of PAR irradiance were well described by the single exponential equation (Lambert–Beer equation, Kirk, 1994):

$$E(\mathrm{PAR}, Z_2) = E(\mathrm{PAR}, Z_1) \times e^{-k(Z_2 - Z_1)},$$

where $E$ (PAR, $Z_2$) and $E$ (PAR, $Z_1$) are PAR irradiances at depths $Z_2$ and $Z_1$ (m), respectively ($Z_2 > Z_1$). Subsequently, the PAR irradiances in the water columns were modelled using exponential regressions (Excel software, dependent variable: PAR irradiance, independent variable: depth). Values of $k$ were obtained from the non-linear regressions of the PAR irradiance profiles only when the determination coefficient ($R^2$) was higher than 0.98. Uncertainty was evaluated by comparing results obtained with two, three, and four depths. The mean maximum difference was 0.6 ± 0.4 $m^{-1}$. Light profiles were then used to calculate the $Z_{eu}$ according to the rule of 1% PAR penetration (Kirk, 1994).

Statistical analyses were conducted with PAST 3.18 software (Hammer, Harper, & Ryan, 2001). Differences between types of aquatic environment (MC, SC, LPC, and LTC) and between hydrological phases (low and high stages) were evaluated according to Kruskal–Wallis test and Mann–Whitney post test with a Bonferroni correction. The Fligner-Killeen test (FK) was used to analyse the effect of the hydrological stage on the spatial heterogeneity by comparing the coefficients of variation of each variable between low and high water stages. The associations of *k* with turbidity, colour, and chlorophyll-*a* were evaluated through generalized linear models (GLM) using the total data set. In addition, each type of environment and each hydrological stage were analysed separately, because the influence of the different optically active components can vary along the MC-floodplain gradient and in relation to the hydrological regime. The models were constructed using the normal distribution and identity function, which is a combination equivalent to ordinary least squares linear regression. Maximum likelihood was calculated by an iteratively reweighted least squares (IRLS) algorithm. The G statistic was estimated as the difference in the deviance between the full model and an additional GLM run where only the intercept was fitted. G is approximately chi-squared with one degree of freedom, giving a value to evaluate the significance of the slope.

Indices $k \times SD$ and $Z_{eu}/SD$ were calculated. Spearman's coefficient (rho) was used to evaluate their relations with the measured variables. The prediction models of $Z_{eu}$ and *k* were run including the total data set. They were based on the mean indices $k \times SD$ and $Z_{eu}/SD$ as well as on linear and potential regressions using SD and the inverse SD as predictor variables. In additon, models were run for each type of environment and each hydrological stage. Differences in the linear models among types of environment and between hydrological stages were evaluated through one-way analysis of covariance. This analysis tests equality of means of a dependent variable (*k* or $Z_{eu}$) adjusted for covariance with a predictor variable (1/SD or SD) and equality of slopes. The feasibility of the different prediction models of *k* and $Z_{eu}$ were compared through their relative root mean square errors (RRMSE), mean relative errors (MRE), and residuals standardized for the magnitude of the expected value (Hammer et al., 2001). Residual normality was assessed through Anderson–Darling test. The median indices $k \times SD$ and $Z_{eu}/SD$ were compared with those proposed in previous studies (Koenings & Edmundson, 1991; Padial & Thomaz, 2008; Poole & Atkins, 1929; Zhang et al., 2012) through Wilcoxon test. In all cases, a *p* value of less than .05 was considered statistically significant.

## 3 | RESULTS

### 3.1 | Spatio-temporal variability in PAR attenuation and related variables

Underwater light climate was highly variable (Figure 2a,b). From the MC towards the most isolated sites, SD, $Z_{eu}$, and chlorophyll-*a* increased, whereas *k*, turbidity, and Turb/Col decreased (Table 1), with

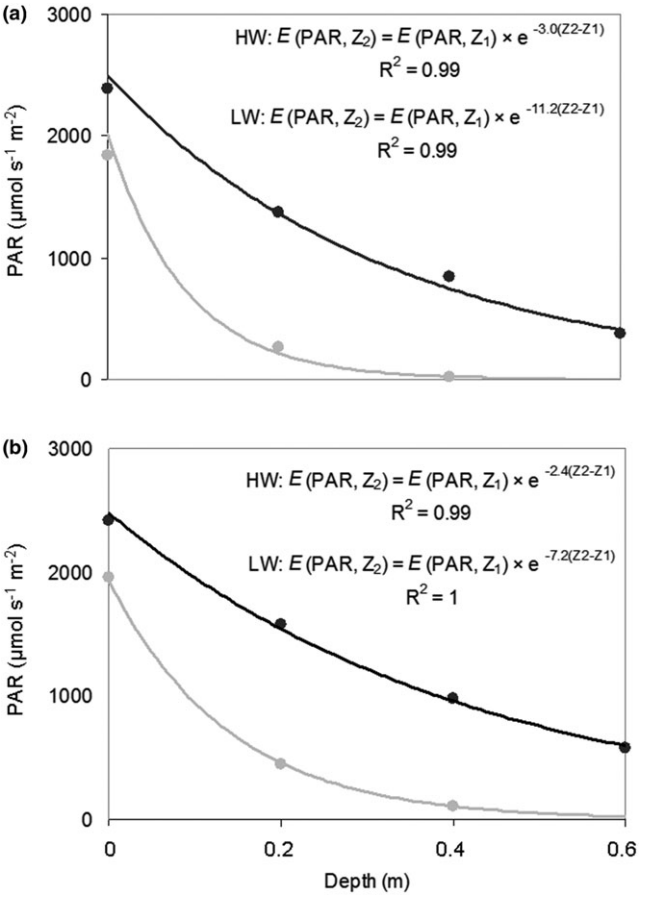


**FIGURE 2** Exponential functions describing vertical profiles of photosynthetically active radiation (PAR) irradiance in the main channel of the Middle Paraná River (a) and a lake temporarily connected to the fluvial system (b) during low-water stage (2014 sampling, light circles) and high water stage (2016 sampling, dark circles). *E* (PAR, $Z_2$) and *E* (PAR, $Z_1$) are PAR irradiances at depths $Z_2$ and $Z_1$, respectively ($Z_2 > Z_1$)

significant differences between lotic environments and LTC (Kruskal–Wallis, $p < .05$). All environments displayed lower *k*, turbidity, Turb/Col and chlorophyll-*a*, and higher colour during high-water stage than low-water stage (Kruskal–Wallis, $p < .05$; Table 1). According to FK test, floods resulted in a significant decrease in the coefficients of variation of chlorophyll-*a* (FK = 67), turbidity (FK = 62), Turb/Col (FK = 74), *k* (FK = 66), and $Z_{eu}$ (FK = 64; $p < .05$).

Turbidity was positively associated with *k* (Figure 3a) considering the whole data set and analysing data separately for each type of environment and/or for each hydrological stage (GLM, $p < .0001$; Table 2). During high-water stage, CDOM and chlorophyll-*a* were also significant explanatory variables of *k* values (Figure 3b,c) considering all environments ($p < .0001$ and $p < .01$, respectively) and for each type of environment ($p < .01$ and $p < .05$, respectively), with the exception of chlorophyll-*a* in MC ($p > .05$). In addition, chlorophyll-*a* was a significant explanatory variable of *k* for LPC and LTC for the whole study period (GLM, $p < .05$; Table 2).

**TABLE 1** Mean values and variation (in brackets) of optical measurements and related variables in the main channel and floodplain environments of the Middle Paraná River sampled between 2013 and 2016

| | Temporal variability | | Spatial variability | | | |
|---|---|---|---|---|---|---|
| | LW | HW | MC | SC | LPC | LTC |
| $k$ ($m^{-1}$) | 6.2[b] (1.3–15.2) | 2.9[a] (1.6–5.6) | 5.4[a] (2.2–15.2) | 4.9[a] (1.6–10.8) | 4.6[a, b] (1.5–11.2) | 3.2[b] (1.3–7.2) |
| $Z_{eu}$ (m) | 1.0[b] (0.3–3.5) | 1.8[a] (0.8–2.8) | 1.1[a] (0.3–2.1) | 1.2[a] (0.4–2.8) | 1.4[a, b] (0.4–3.0) | 1.8[b] (0.6–3.5) |
| SD (cm) | 30[b] (10–124) | 64[a] (23–140) | 32[a] (10–78) | 42 [a] (11–114) | 53[a, b] (10–128) | 61[b] (16–140) |
| $k \times$ SD | 1.4[b] (0.8–2.6) | 1.6[a] (0.8–2.9) | 1.3 (0.8–1.7) | 1.5 (0.9–2.8) | 1.6 0.8–2.9) | 1.6 (0.9–2.7) |
| $Z_{eu}$/SD | 3.6[b] (1.7–6.1) | 3.1[a] (1.6–5.5) | 3.7 (2.7–5.5) | 3.3 (1.7–5.0) | 3.3 (1.6–6.1) | 3.3 (1.7–5.4) |
| Turb (FTU) | 70[b] (7–225) | 21[a] (6–52) | 58[a] (12–178) | 51[a] (8–225) | 44 [a, b] (6–137) | 26[b] (7–65) |
| Col (mg $L^{-1}$ Pt-Co) | 38[b] (12–85) | 59[a] (31–95) | 50 (17–95) | 50 (13–84) | 49 (12–93) | 48 (17–78) |
| Turb/Col | 25[b] (3–114) | 4[a] (1–10) | 19 (2–100) | 16 (2–108) | 14 (1–114) | 6 (2–25) |
| Chl-*a* (μg $L^{-1}$) | 8.1[b] (0.7–47.3) | 3.7[a] (1.3–10.3) | 3.1[a] (0.8–7.4) | 4.9[a] (0.7–39.5) | 4.5 [a, b] (1.3–12.6) | 9.8[b] (1.4–47.3) |

*Note*. Different letters indicate significant differences between hydrological stages and between types of environment, according to Kruskal–Wallis test and Mann–Whitney post test corrected by Bonferroni ($p < .05$).

Abbreviations: Chl-*a*, chlorophyll-*a*; Col, colour; HW, high-water stage; *k*, attenuation coefficient of photosynthetically active radiation; LPC, lakes permanently connected to the fluvial system; LTC, lakes temporarily connected to the fluvial system; LW, low-water stage; SC, secondary channels; SD, Secchi disc depth; Turb, turbidity; $Z_{eu}$, euphotic zone depth.

## 3.2 | Estimation of k and $Z_{eu}$ by using SD

The indices $k \times$ SD and $Z_{eu}$/SD showed significant associations with SD (rho = 0.50 and −0.50), turbidity (rho = −0.43 and 0.43), and Turb/Col (rho = −0.41 and 0.41, respectively; $p < .001$). The index $k \times$ SD displayed higher values on the floodplain than in the MC and during high-water stage than low-water stage; whereas the index $Z_{eu}$/SD showed an inverse behaviour (Kruskal–Wallis, $p < .05$ for differences between stages).

Differences among linear regressions to predict $k$ and $Z_{eu}$ through the inverse SD and SD, respectively, were not significant for the type of environment at any time scale (low-water stage, high-water stage, and the whole period; analysis of covariance, test for equality of means of $y$ adjusted for covariance with $x$ and test for equality of slopes: $p > .05$). In contrast, regressions showed significant differences between hydrological stages including the data for all environments (test for equality of means of $y$ adjusted for covariance with $x$: $p < .05$, F = 4.4 and F = 4.6 for the regressions to predict $k$ and $Z_{eu}$, respectively). In addition, slopes of linear regressions to predict $Z_{eu}$ through SD showed significant differences between hydrological stages including the data for all environments ($p < .0001$, F = 25.64), for SC ($p < .05$, F = 4.45), and for LTC ($p < 0.05$, F = 5.86).

The RRMSE and MRE were 34.4% and 27.3% for the model to predict $k$ from the mean $k \times$ SD for the whole data set (1.5) and 33.2% and 27.1% when using the mean $k \times$ SD for low-water (1.4) and high-water (1.6) stages. Considering the whole data set, the results of the linear regression model ($k = 1.04 \times 1/\text{SD} + 1.05$; $R^2 = 0.74$; $N = 104$; Figure 4 a) showed RRMSE and MRE values of 26.0% and 20.2%; whereas the results of the potential regression model ($k = 1.89 \times \text{SD}^{-0.73}$; $R^2 = 0.80$; $N = 104$; Figure 4b) showed RRMSE and MRE values of 25.4% and 20.0%, respectively. When using specific linear regressions for the low-water stage ($k = 0.96 \times 1/\text{SD} + 1.67$, $R^2 = 0.61$, $N = 52$) and the high-water stage ($k = 0.86 \times 1/\text{SD} + 1.18$, $R^2 = 0.70$, $N = 52$; Figure 4a), the results showed RRMSE and MRE values of 27.7% and 20.5%, respectively. When using specific potential regressions for the low-water stage ($k = 1.76 \times \text{SD}^{-0.80}$, $R^2 = 0.74$, $N = 52$) and the high-water stage ($k = 2.04 \times \text{SD}^{-0.53}$, $R^2 = 0.68$, $N = 52$; Figure 4b), the results showed RRMSE and MRE values of 23.8% and 18.7%, respectively. In all the models, predictions were biased at high estimated values (Figure .5a–c). The Anderson–Darling test indicated that residuals of the linear and the potential models were not normally distributed ($p < .001$; A–D = 2.5 and 2.4, respectively).

In contrast, the RRMSE and MRE were 36.4% and 27.9% for the model to predict $Z_{eu}$ from the mean $Z_{eu}$/SD for the whole data set (3.3) and 35.5% and 27.3% when using the mean $Z_{eu}$/SD for low-water (3.6) and high-water (3.1) stages. Considering the whole data set, the results of the linear regression model ($Z_{eu} = 1.81 \times \text{SD} + 0.53$, $R^2 = 0.72$, $N = 104$; Figure 4c) showed RRMSE and MRE values of 36.7% and 25.9%; whereas the results of the potential regression model ($Z_{eu} = 2.41 \times 1/\text{SD}^{-0.73}$, $R^2 = 0.80$, $N = 104$; Figure 4d) showed RRMSE and MRE values of 27.0% and 20.6%, respectively. When using specific linear regressions for the low-water stage ($Z_{eu} = 2.59 \times \text{SD} + 0.23$, $R^2 = 0.77$, $N = 52$) and the high-water stage (linear relation: $Z_{eu} = 1.29 \times \text{SD} + 0.93$, $R^2 = 0.61$, $N = 52$; Figure 4 c), the results showed RRMSE and MRE values of 27.3% and 20.7%. When using specific potential regressions for the low-water stage ($Z_{eu} = 2.62 \times 1/\text{SD}^{-0.80}$, $R^2 = 0.74$, $N = 52$) and the high-water stage ($Z_{eu} = 2.26 \times 1/\text{SD}^{-0.53}$, $R^2 = 0.68$, $N = 52$; Figure 4d), the results showed RRMSE and MRE values of 25.0% and 19.0%, respectively. The models to predict $Z_{eu}$ showed lower standardized residuals than the models to predict $k$. Residuals of the potential model were more randomly distributed around zero than residuals of the model based on the mean index $Z_{eu}$/SD and residuals of the linear model (Figure .5d–f). The Anderson–Darling test indicated that residuals of the model based on the mean index $Z_{eu}$/SD were not normally distributed ($p < .05$, A–D = 1.0).

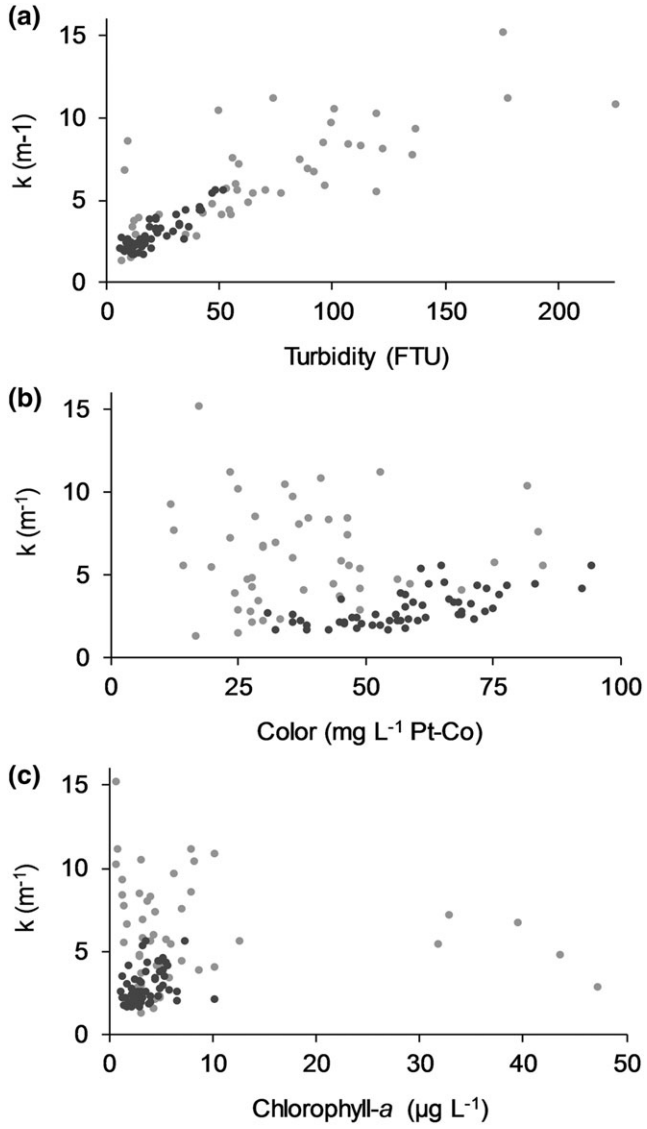


**FIGURE 3** Scatter plot of *k* versus turbidity (a), colour (b), and chlorophyll-*a* (c). The analyses considered low-water stage (light circles) and high-water stage (dark circles)

In agreement with Wilcoxon test, the median index $k \times SD$ (1.4) differed significantly from the values proposed by Poole and Atkins (1929; 1.7, W = 3826), Padial and Thomaz (2008; 2.3, W = 5229), and Koenings and Edmundson (1991; 2.7, 1.9, and 0.9, W = 5,360, 4,554, and 5,412, respectively; $p < .001$) but not from the value proposed by Zhang et al. (2012) for turbid waters (1.4; $p > .05$). The median index $Z_{eu}/SD$ (3.2) differed significantly from the values proposed by Koenings and Edmundson (1991; 1.8, 2.4, and 4.9, W = 5,420, 4,892, and 5,340, respectively; $p < .001$).

## 4 | DISCUSSION

The estimation of *k* and $Z_{eu}$ through SD in a turbid river-floodplain system was sensitive to the effects of temporal variations as expected due to the influence of the hydrological regime. In this sense, our hypothesis was partially validated because we did not find an effect on *k* and $Z_{eu}$ estimation due to changes in optically active components along the spatial gradient.

### 4.1 | Spatio-temporal variability in PAR attenuation and related variables

The decreasing trends in turbidity and *k* as well as the increasing trends in chlorophyll-*a* and SD from the fluvial system towards the most isolated floodplain water bodies were in agreement with previous research (Cardoso, Roland, Loverde-Oliveira, & Huszar, 2012; Izaguirre, O'Farrell, & Tell, 2001; Maine et al., 2004; Mayora et al., 2013; O'Farrell, Izaguirre, & Vinocur, 1996; Unrein, 2002; Zalocar de Domitrovic et al., 2007). The higher similarities in light climate along the spatial gradient during high-water stage than low-water stage were consistent with the general pattern of flood homogenization, which was derived from increased regional driving forces due to the high hydrological connectivity (Thomaz et al., 2007). During low-water stage, in contrast, local catchment features such as water column depth, morphometry, and land use become important factors that increase the variability in inputs and outputs of optically active components (Fergus, Soranno, Cheruvelil, & Bremigan, 2011; Thomaz et al., 2007).

The high turbidity of the Middle Paraná River system is a consequence of the high concentration of suspended sediments (Pedrozo & Bonetto, 1989). Hydrological and sedimentological regimes depend on different subcatchments within the Paraná drainage basin. Whereas most of the water discharge comes from the Upper Paraná River, most of the suspended sediments come from the Bermejo River, an Andean tributary (Amsler & Drago, 2009). Hence, hydrological and sedimentological regimes were not coupled. The 2014 sampling (low-water stage) coincided with the inflow of waters enriched with suspended solids supplied by the Bermejo River due to the arrival of the rainy season in their Andean headwaters. Therefore, the highest values of turbidity were observed during low-water stage, mainly in the MC and its anabranches. Because the LTC to the fluvial system were isolated during the arrival of the sediment peak at the MC, they did not receive inputs of solids from the Bermejo River. However, the highest values of turbidity also occurred during low-water stage in the LTC, probably due to phytoplankton development and sediment resuspension through wind action (García de Emiliani, 1997; Liu et al., 2013; Zalocar de Domitrovic, 2003). Given the controlling effect of particulate components on temporal and spatial variability in PAR attenuation, *k* was the highest during low-water stage (mean $k = 6.2\ m^{-1}$), with values up to $15.2\ m^{-1}$ in the MC. These values are among the highest reported for freshwater environments (Arst, Noges, Noges, & Paavel, 2008; Davies-Colley & Nagels, 2008; Padial & Thomaz, 2008; Squires & Lesack, 2003).

Lower PAR attenuation during high-water stage could have increased the effects of different optically active components. In this respect, the effect of chlorophyll-*a* on PAR attenuation variability was more noticeable during the floods, although its concentration

**TABLE 2** Results of the generalized linear models to analyse relations of *k* values (dependent variable) with turbidity, colour, and chlorophyll-*a* (explanatory variables), considering the whole data set and grouping data according to hydrological stages (LW = low water stage, HW = high water stage) and/or types of environment (MC = main channel and anabranches, SC = secondary channels, LPC = lakes permanently connected to the fluvial system, LTC = lakes temporarily connected to the fluvial system)

| | Phi | Slope | Intercept | G | *p* (slope = 0) |
|---|---|---|---|---|---|
| Whole data set (*N* = 104) | | | | | |
| Turbidity | 0.02 | 0.519 | −0.175 | 240.9 | <0.0001 |
| LW (*N* = 52) | | | | | |
| Turbidity | 0.03 | 0.414 | 0.048 | 49.4 | <0.0001 |
| HW (*N* = 52) | | | | | |
| Turbidity | 0.01 | 0.485 | −0,168 | 108.2 | <0.0001 |
| Colour | 0.01 | 0.842 | −1.037 | 35.8 | <0.0001 |
| Chlorophyll-*a* | 0.02 | 0.250 | 0.310 | 7.3 | <0.01 |
| MC, all period (*N* = 16) | | | | | |
| Turbidity | 0.01 | 0.616 | −0.335 | 64.4 | <0.0001 |
| MC, LW (*N* = 8) | | | | | |
| Turbidity | 0.01 | 0.515 | −0.108 | 20.8 | <0.0001 |
| MC, HW (*N* = 8) | | | | | |
| Turbidity | 0.01 | 0.542 | −0.265 | 9.0 | <0.01 |
| Colour | 0.01 | 0.737 | −0.829 | 5.3 | <0.05 |
| SC, all period (*N* = 34) | | | | | |
| Turbidity | 0.02 | 0.463 | −0.074 | 60.4 | <0.0001 |
| SC, LW (*N* = 17) | | | | | |
| Turbidity | 0.02 | 0.282 | 0.301 | 11.8 | <0.001 |
| SC, HW (*N* = 17) | | | | | |
| Turbidity | 0.01 | 0.569 | −0.271 | 35.3 | <0.0001 |
| Colour | 0.01 | 1.107 | −1.499 | 14.8 | <0.001 |
| Chlorophyll-*a* | 0.01 | 0.538 | 0.170 | 9.0 | <0.01 |
| LPC, all period (*N* = 28) | | | | | |
| Turbidity | 0.03 | 0.510 | −0.138 | 42.7 | <0.0001 |
| Chlorophyll-*a* | 0.06 | 0.483 | 0.298 | 5.1 | <0.05 |
| LPC, LW (*N* = 14) | | | | | |
| Turbidity | 0.01 | 0.722 | −0.522 | 39.9 | <0.0001 |
| LPC, HW (*N* = 14) | | | | | |
| Turbidity | 0.01 | 0.457 | −0.119 | 19.7 | <0.0001 |
| Colour | 0.01 | 1.063 | −1.431 | 11.2 | <0.001 |
| Chlorophyll-*a* | 0.02 | 0.488 | 0.183 | 5.9 | <0.05 |
| LTC, all period (*N* = 26) | | | | | |
| Turbidity | 0.01 | 0.510 | −0.206 | 77.7 | <0.0001 |
| Chlorophyll-*a* | 0.03 | 0.275 | 0.252 | 12.3 | <0.001 |
| LTC, LW (*N* = 13) | | | | | |
| Turbidity | 0.01 | 0.551 | −0.262 | 24.6 | <0.0001 |
| Colour | 0.03 | 0.990 | −0.979 | 6.3 | <0.05 |
| Chlorophyll-*a* | 0.04 | 0.342 | 0.241 | 5.5 | <0.05 |
| LTC, HW (*N* = 13) | | | | | |
| Turbidity | 0.01 | 0.449 | −0.136 | 28.7 | <0.0001 |

(Continues)

**TABLE 2** (Continued)

| | Phi | Slope | Intercept | G | *p* (slope = 0) |
|---|---|---|---|---|---|
| Colour | 0.01 | 0.842 | −1.075 | 8.3 | <0.01 |
| Chlorophyll-*a* | 0.02 | 0.434 | 0.167 | 5.2 | <0.05 |

*Note*. Only variables positively and significantly associated with *k* are shown. Data were log-transformed.

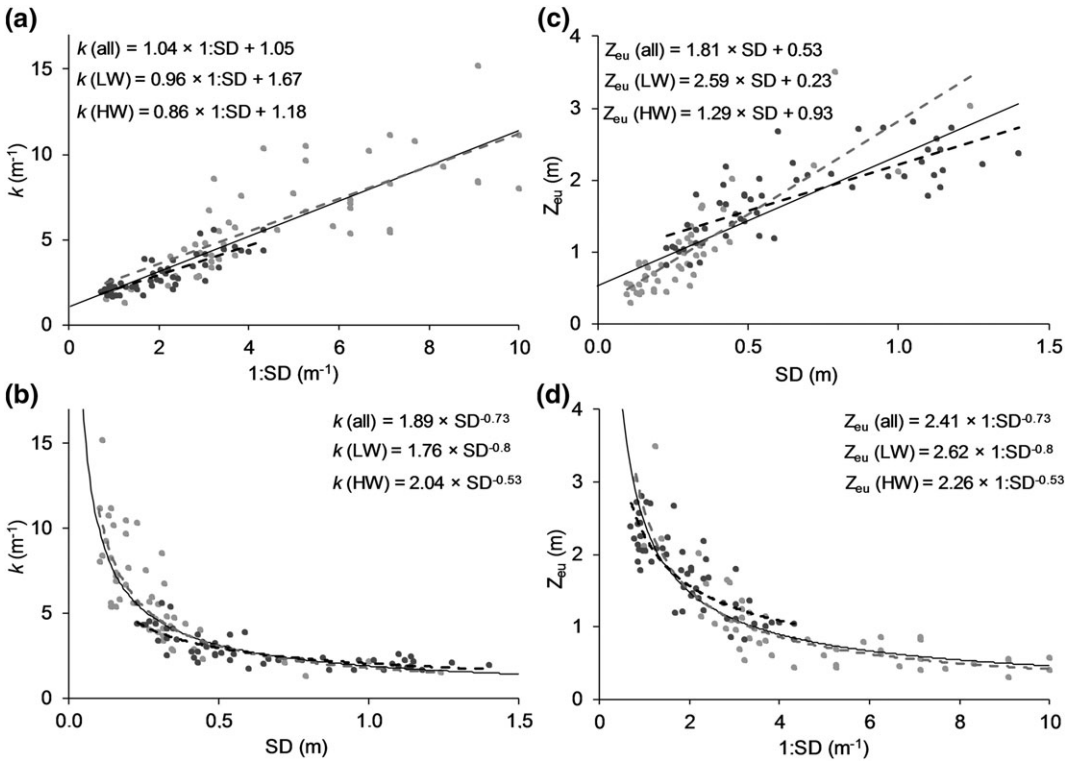


**FIGURE 4** Linear (a, b) and non-linear models (c, d) for estimation of photosynthetically active radiation attenuation coefficient (*k*) and euphotic zone depth ($Z_{eu}$) using Secchi disc. The models were generated by considering the whole data set (black entire lines), low-water stage (light circles and dashed lines), and high-water stage (dark circles and dashed lines)

was lower than during low-water stage. The effect of CDOM was also more noticeable during high-water stage than low-water stage, which would have been favoured by increasing CDOM concentration due to its input from flooded areas (Costa et al., 2013; Mladenov, McKnight, Wolski, & Ramberg, 2005; Sieczko & Peduzzi, 2014).

## 4.2 | Estimation of k and $Z_{eu}$ through SD

Indices *k* × SD and $Z_{eu}$/SD proposed for clear environments (Koenings & Edmundson, 1991; Padial & Thomaz, 2008; Poole & Atkins, 1929) should not be applied to turbid environments because of the significant differences between them. Even using the indices developed specifically for the turbid system under study, RRMSE and MRE were markedly higher for models based on indices than for regression models. On the other hand, linear regressions showed higher errors than non-linear regressions, similarly to that observed in previous studies (Padial & Thomaz, 2008; Zhang et al., 2012). Therefore, we propose the use of non-linear models to estimate underwater light climate through SD.

The significant differences in models between low and high-water stages were probably associated with the changes in scattering and absorption of PAR because the balance between both processes influences the associations between SD and *k* and between SD and $Z_{eu}$ (Effler, 1985; Koenings & Edmundson, 1991). As a result, predictions were improved by using a model for each hydrological stage instead of a single model for the whole period. Therefore, we propose considering the use of a specific model for each hydrological stage in turbid river-floodplain systems.

All the models to predict *k* showed markedly higher residuals when the values of the estimated variable increased, especially during low-water stage, probably due to the higher spatial heterogeneity of the optically active components affecting the relation between SD and *k*. In this respect, when estimations of *k* were above 4 $m^{-1}$, slight changes in the independent variable led to greater changes in the predicted values. Therefore, caution must be taken when making estimations exceeding this value. Considering that the highest accuracy was recorded for predicting $Z_{eu}$, and that ecological implications of light climate depend on $Z_{eu}$:depth ratio, we suggest that SD should be used to estimate $Z_{eu}$ instead of *k* in ecological studies.

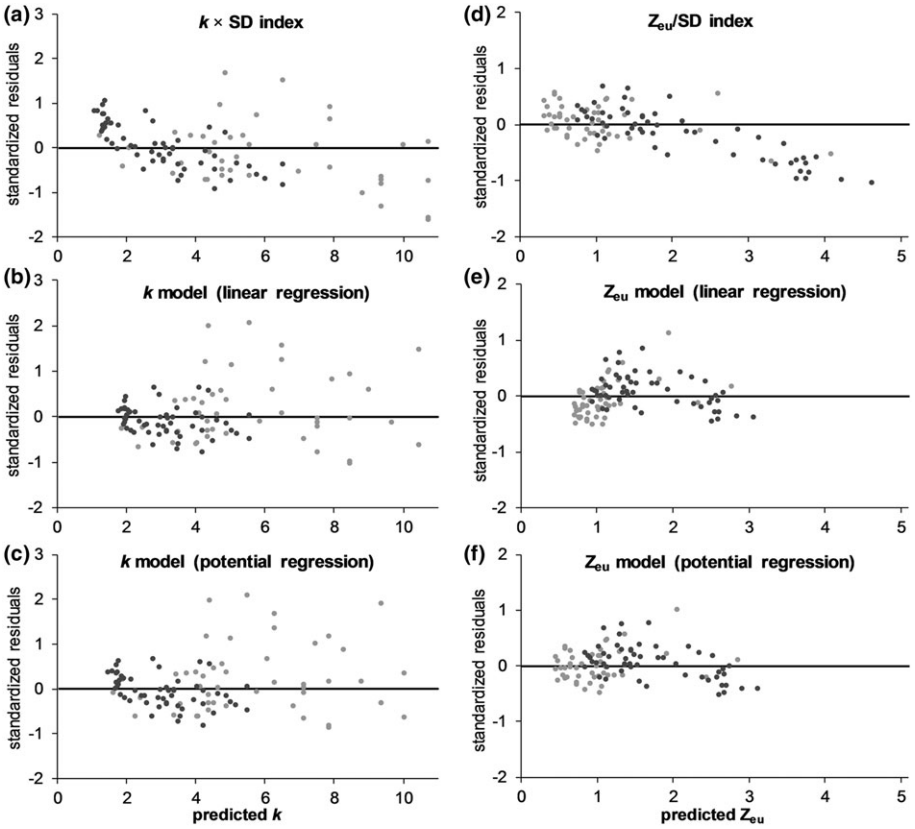


**FIGURE .5** Raw residuals of indices and regression models generated to estimate photosynthetically active radiation attenuation coefficient (*k*; a–c) and euphotic zone depth ($Z_{eu}$; d–f). Residuals were calculated as the observed minus the predicted values. The analyses considered the whole data set (black entire lines), low-water stage (light circles and dashed lines), and high-water stage (dark circles and dashed lines)

## 5 | CONCLUSIONS

The associations between SD and *k*, and between SD and $Z_{eu}$, were significantly affected by temporal variations in the hydrological conditions, but the effect of variability in the spatial gradient was insignificant. The greatest prediction accuracy of underwater light climate was observed when estimating $Z_{eu}$ through specific non-linear regression models for each hydrological stage (low water: $Z_{eu} = 2.62 \times 1/SD^{-0.80}$; high water: $Z_{eu} = 2.26 \times 1/SD^{-0.53}$). Therefore, their use should be considered to estimate underwater light climate through SD in turbid river-floodplain systems. Our results highlight the importance of considering the temporal variations in models to estimate *k* and $Z_{eu}$, particularly for aquatic ecosystems which present marked temporal changes in optically active components. Finally, future research should evaluate if the models proposed for the flood periods are appropriate to estimate *k* and $Z_{eu}$ when this hydrological phase overlaps with the arrival of the sediment peak.

## ACKNOWLEDGEMENTS

We thank Cristian Debonis, Esteban Creus, and Marcelo Piacenza for their field assistance. Financial support was granted by Consejo Nacional de Investigaciones Científicas y Técnicas (CONICET) and Agencia Nacional de Promoción Científica y Tecnológica (PICT 2010-2350, PI Devercelli M.; PICT 2012-2095, PI Marchese M.). Authors thank the Argentinian public politics during the period 2003 to 2015 for supporting scientific and technological development. Currently, the Argentina's science and technology system is about to be paralysed due to budget cuts. We urge the government of Argentina to revert these policies.

## DATA AVAILABILITY STATEMENT (DAS)

Raw data were generated at Instituto Nacional de Limnología (INALI-CONICET-UNL). Derived data supporting the findings of this study are available from the corresponding author G. Mayora on request.

## ORCID

*Gisela Mayora* https://orcid.org/0000-0003-2839-2803

## REFERENCES

Amsler, M. L., & Drago, E. C. (2009). A review of the suspended sediment budget at the confluence of the Paraná and Paraguay Rivers. *Hydrological Processes*, *23*, 3230–3235. https://doi.org/10.1002/hyp.7390

Amsler, M. L., Drago, E. C., & Paira, A. R. (2007). Fluvial sediments: Main channel and floodplain interrelationships. In M. H. Iriondo, J. C. Paggi, & M. J. Parma (Eds.), *Middle Parana River: Limnology of a subtropical wetland* (pp. 123–142). Berlin, Germany: Springer-Verlag.

APHA (2005). *Standard methods for the examination of water and wastewaters* (21 st). Washington: American Public Health Association.

Arst, H., Noges, T., Noges, P., & Paavel, B. (2008). Relations of phytoplankton in situ primary production, chlorophyll concentration and underwater irradiance in turbid lakes. *Hydrobiologia*, *599*, 169–176. https://doi.org/10.1007/s10750-007-9213-z

Bonetto, C., de Cabo, L., Gabellone, N., Vinocur, A., Donadelli, J., & Unrein, F. (1994). Nutrient dynamics in the deltaic floodplain of the Lower Paraná River. *Archiv für Hydrobiologie*, *131*, 277–295.

Campodonico, V. A., García, M. G., & Pasquini, A. I. (2016). The geochemical signature of suspended sediments in the Parana River basin: Implications for provenance, weathering and sedimentary recycling. *Catena*, *143*, 201–214. https://doi.org/10.1016/j.catena.2016.04.008

Cardoso, S. J., Nabout, J. C., Farjalla, V. F., Lopes, P. M., Bozelli, R. L., Huszar, V. L. M., & Roland, F. (2017). Environmental factors driving phytoplankton taxonomic and functional diversity in Amazonian floodplain lakes. *Hydrobiologia*, *802*, 115–130. https://doi.org/10.1007/s10750-017-3244-x

Cardoso, S. J., Roland, F., Loverde-Oliveira, S. M., & Huszar, V. L. M. (2012). Phytoplankton abundance, biomass and diversity within and between Pantanal wetland habitats. *Limnologica*, *42*, 235–241. https://doi.org/10.1016/j.limno.2012.01.002

Costa, M. P. F., Novo, E. M. L. M., & Telmer, K. H. (2013). Spatial and temporal variability of light attenuation in large rivers of the Amazon. *Hydrobiologia*, *702*, 171–190. https://doi.org/10.1007/s10750-012-1319-2

Davies-Colley, R. J., & Nagels, J. W. (2008). Predicting light penetration into river waters. *Journal of Geophysical Research*, *113*, G03028.

Devercelli, M., Scarabotti, P., Mayora, G., Schneider, B., & Giri, F. (2016). Unravelling the role of determinism and stochasticity in structuring the phytoplanktonic metacommunity of the Paraná River Floodplain. *Hydrobiologia*, *764*, 139–156. https://doi.org/10.1007/s10750-015-2363-5

Drago, E. C. (2007). The physical dynamics of the river-lake floodplain system. In M. H. Iriondo, J. C. Paggi, & M. J. Parma (Eds.), *Middle Parana River: Limnology of a subtropical wetland* (pp. 83–122). Berlin, Germany: Springer-Verlag.

Effler, S. W. (1985). Attenuation versus Transparency. *Journal of Environmental Engineering*, *111*, 448–459. https://doi.org/10.1061/(ASCE)0733-9372(1985)111:4(448)

Fergus, C. E., Soranno, P. A., Cheruvelil, K. S., & Bremigan, M. T. (2011). Multiscale landscape and wetland drivers of lake total phosphorus and water color. *Limnology and Oceanography*, *56*, 2127–2146. https://doi.org/10.4319/lo.2011.56.6.2127

García de Emiliani, M. O. (1997). Effects of water level fluctuations on phytoplankton in a river-floodplain lake system (Paraná River, Argentina). *Hydrobiologia*, *357*, 1–15. https://doi.org/10.1023/A:1003149514670

Hammer, Ø., Harper, D. A. T., & Ryan, P. D. (2001). PAST: Paleontological Statistics Software Package for Education and Data Analysis. *Palaeontologia Electronica*, *4*, 9.

Izaguirre, I., O'Farrell, I., & Tell, G. (2001). Variation in phytoplankton composition and limnological features in a water–water ecotone of the Lower Paraná Basin (Argentina). *Freshwater Biology*, *46*, 63–74.

Kirk, J. T. O. (Ed.) (1994). *Light and photosyntesis in aquatic ecosystems*. Cambridge: Cambridge University Press. https://doi.org/10.1017/CBO9780511623370

Koenings, J. P., & Edmundson, J. A. (1991). Secchi disk and photometer estimates of light regimes in Alaskan lakes: Effects of yellow color and turbity. *Limnology and Oceanography*, *36*, 91–105. https://doi.org/10.4319/lo.1991.36.1.0091

Liu, X., Zhang, Y., Yin, Y., Wang, M., & Qin, B. (2013). Wind and submerged aquatic vegetation influence bio-optical properties in large shallow Lake Taihu, China. *Journal of Geophysical Research: Biogeosciences*, *118*, 713–727. https://doi.org/10.1002/jgrg.20054

Maine, M. A., Suñe, N. L., & Bonetto, C. (2004). Nutrient concentrations in the Middle Paraná River: Effect of the floodplain lakes. *Archiv für Hydrobiologie*, *160*, 85–103. https://doi.org/10.1127/0003-9136/2004/0160-0085

Mayora, G., Devercelli, M., & Frau, D. (2016). Spatial variability of chromophoric dissolved organic matter in a large floodplain river: control factors and relations with phytoplankton during a low water period. *Ecohydrology*, *9*, 487–497. https://doi.org/10.1002/eco.1651

Mayora, G., Devercelli, M., & Giri, F. (2013). Spatial variability of chlorophyll-a and abiotic variables in a river–floodplain system during different hydrological phases. *Hydrobiologia*, *717*, 51–63. https://doi.org/10.1007/s10750-013-1566-x

Mladenov, N., McKnight, D. M., Wolski, P., & Ramberg, L. (2005). Effects of annual flooding on dissolved organic carbon dynamics within a pristine wetland, the Okavango Delta, Botswana. *Wetlands*, *25*, 622–638. https://doi.org/10.1672/0277-5212(2005)025[0622:EOAFOD]2.0.CO;2

O'Farrell, I., Izaguirre, I., & Vinocur, A. (1996). Phytoplankton ecology of the Lower Paraná River (Argentina). Large Rivers. *Archiv für Hydrobiologie Supplement*, *115*, 75–89.

Padial, A. A., & Thomaz, S. M. (2008). Prediction of the light attenuation coefficient through the Secchi disk depth: Empirical modeling in two large Neotropical ecosystems. *Limnology*, *9*, 143–151. https://doi.org/10.1007/s10201-008-0246-4

Pedrozo, F. L., & Bonetto, C. A. (1989). Influence of river regulation on Nitrogen and Phosphorus mass transport in a large South american river. *River Research and Applications*, *4*, 59–70.

Piedade, M. T. F., Junk, W., D'Ângelo, S. A., Wittmann, F., Schöngart, J., Barbosa, K. M. N., & Lopes, A. (2010). Aquatic herbaceous plants of the Amazon floodplains: state of the art and research hended. *Acta Limnologica Brasiliensia*, *22*, 165–178. https://doi.org/10.4322/actalb.02202006

Pineda, A., Moresco, G. A., Magro de Paula, A. C., Nogueira, L. M., Iatskiu, P., Rodrigues de Souza, Y., … Rodrigues, L. C. (2017). Rivers affect the biovolume and functional traits of phytoplankton in floodplain lakes. *Acta Limnologica Brasiliensia*, *29*, e113.

Poole, H. H., & Atkins, W. R. G. (1929). Photoelectric measurements of submarine illumination throughout the year. *Journal of the Marine Biological Association of the United Kingdom*, *16*, 297–324. https://doi.org/10.1017/S0025315400029829

Roberto, M. C., Santana, N. F., & Thomaz, S. M. (2009). Limnology in the Upper Paraná River floodplain: Large-scale spatial and temporal patterns, and the influence of reservoirs. *Brazilian Journal of Biology*, *69*, 717–725. https://doi.org/10.1590/S1519-69842009000300025

Rügner, H., Schwientek, M., Beckingham, B., Kuch, B., & Grathwohl, P. (2013). Turbidity as a proxy for total suspended solids (TSS) and particle facilitated pollutant transport in catchments. *Environmental Earth Sciences*, *69*, 373–380. https://doi.org/10.1007/s12665-013-2307-1

Sabattini, R. A., & Lallana, V. H. (2007). Aquatic macrophytes). In M. H. Iriondo, J. C. Paggi, & M. J. Parma (Eds.), *Middle Parana River: Limnology of a subtropical wetland* (pp. 205–226). Berlin, Germany: Springer-Verlag. https://doi.org/10.1007/978-3-540-70624-3_8

Shi, K., Zhang, Y., Liu, X., Wang, M., & Qin, B. (2014). Remote sensing of diffuse attenuation coefficient of photosynthetically active radiation in Lake Taihu using MERIS data. *Remote Sensing of Environment*, *140*, 365–377. https://doi.org/10.1016/j.rse.2013.09.013

Sieczko, A., & Peduzzi, P. (2014). Origin, enzymatic response and fate of dissolved organic matter during flood and non-flood conditions in a river-floodplain system of the Danube (Austria). *Aquatic Sciences*, *76*, 115–129. https://doi.org/10.1007/s00027-013-0318-3

Squires, M. M., & Lesack, L. F. W. (2003). Spatial and temporal patterns of light attenuation among lakes of the Mackenzie Delta. *Freshwater Biology*, *48*, 1–20. https://doi.org/10.1046/j.1365-2427.2003.00960.x

Thomaz, S. M., Bini, L. M., & Bozelli, R. L. (2007). Floods increase similarity among aquatic habitats in river-floodplain systems. *Hydrobiologia*, *579*, 1–13. https://doi.org/10.1007/s10750-006-0285-y

Tockner, K., Pusch, M., Borchardt, D., & Lorang, M. S. (2010). Multiple stressors in coupled river–floodplain ecosystems. *Freshwater Biology*, *55*, 135–151. https://doi.org/10.1111/j.1365-2427.2009.02371.x

Unrein, F. (2002). Changes in phytoplankton community along a transversal section of the Lower Parana floodplain, Argentina. *Hydrobiologia*, *468*, 123–134. https://doi.org/10.1023/A:1015254320940

Zalocar de Domitrovic, Y. (2003). Effect of fluctuations in water level on phytoplankton development in three lakes of the Paraná river floodplain (Argentina). *Hydrobiologia*, *510*, 175–193. https://doi.org/10.1023/B:HYDR.0000008643.50105.4b

Zalocar de Domitrovic, Y., Devercelli, M., & García de Emiliani, M. O. (2007). Phytoplankton. In M. H. Iriondo, J. C. Paggi, & M. J. Parma (Eds.), *Middle Parana River: Limnology of a subtropical wetland* (pp. 177–203). Berlin, Germany: Springer-Verlag. https://doi.org/10.1007/978-3-540-70624-3_7

Zanco, B. F., Pineda, A., Bortolini, J. C., Jati, S., & Rodrigues, L. C. (2017). Phytoplankton functional groups indicators of environmental conditions in floodplain rivers and lakes of the Paraná Basin. *Acta Limnologica Brasiliensia*, *29*, e119.

Zhang, Y., Liu, X., Qin, B., Shi, K., Deng, J., & Zhou, Y. (2016). Aquatic vegetation in response to increased eutrophication and degraded light climate in Eastern Lake Taihu: Implications for lake ecological restoration. *Scientific Reports*, *6*, 23867. https://doi.org/10.1038/srep23867

Zhang, Y., Liu, X., Yin, Y., Wang, M., & Qin, B. (2012). Predicting the light attenuation coefficient through Secchi disk depth and beam attenuation coefficient in a large, shallow, freshwater lake. *Hydrobiologia*, *693*, 29–37. https://doi.org/10.1007/s10750-012-1084-2

Zhang, Y., Zhang, B., Ma, R., Feng, S., & Le, C. (2007). Optically active substances and their contributions to the underwater light climate in Lake Taihu, a large shallow lake in China. *Fundamental and Applied Limnology/Archiv für Hydrobiologie*, *170*, 11–19. https://doi.org/10.1127/1863-9135/2007/0170-0011

**How to cite this article:** Mayora G, Devercelli M. Spatio-temporal variability in underwater light climate in a turbid river-floodplain system: Driving factors and estimation using Secchi disc. *River Res Applic*. 2019;1–11. https://doi.org/10.1002/rra.3429